# Tuned mass damper for self-excited vibration control: optimization involving nonlinear aeroelastic effect

Mingjie Zhang[a], Fuyou Xu[b, *]

[a]*Department of Structural Engineering, Norwegian University of Science and Technology, 7491, Trondheim, Norway*

[b]*School of Civil Engineering, Dalian University of Technology, 116024, Dalian, China*

**Abstract:** The conventional target for self-excited galloping/flutter control of a civil structure often focuses on the critical wind speed. In the present work, a nonlinear control target is introduced, i.e., to ensure that the vibration amplitude is lower than a threshold value (pre-specified according to the expected structural performance) before a target wind speed. Unlike the conventional control target, the nonlinear one can take into account the underlying large-amplitude vibrations before the critical state and/or the structural safety redundancy after the critical state. To obtain the most economical TMD parameters that enable the nonlinear target, an optimization procedure involving nonlinear aeroelastic effect is developed for galloping control based on the quasi-steady aeroelastic force model, and for flutter control based on a nonlinear unsteady model. Three numerical examples involving the galloping/flutter control of different cross-sections are analyzed to demonstrate the different results designed by the conventional and nonlinear targets. It is demonstrated that the nonlinear target and optimization procedure can lead to more economical design results than the conventional ones in the galloping/flutter control for a structure with relatively large post-critical safety redundancy, and they are more reliable than the conventional ones for a structure that may experience large-amplitude vibrations before the critical wind speed. These superiorities of the nonlinear control target and new optimization procedure suggest that they may be utilized in the TMD parameter optimization for galloping/flutter control of structures in a wide domain of engineering fields.

**Keywords:** Vibration control; Nonlinear Aeroelasticity; Tuned mass damper; Galloping; Flutter

* Corresponding Author.
*E-mail addresses*: mingjie.zhang@ntnu.no (M.J. Zhang), fuyouxu@dlut.edu.cn (F.Y. Xu)

## 1. Introduction

Slender flexible structures may be susceptible to various types of wind-induced vibrations, among which the most dangerous ones are self-excited galloping and flutter. Tuned mass dampers (TMDs) have been widely utilized to control these self-excited instabilities due to their simplicity, effectiveness, and relatively low cost. The performance of a TMD is very sensitive to its mass, stiffness, and damping properties. An optimization procedure is generally required to determine the optimal TMD parameters that enable the control target. In the context of galloping/flutter control, the conventional target is to ensure the critical wind speed to be higher than a target value, e.g., for a long-span bridge, the critical flutter wind speed should be higher than a checking wind speed determined according to the wind environment at the bridge site (CCCC Highway Consultants 2004). Since the linear critical state of an aeroelastic system is not affected by the nonlinear part of the aeroelastic force, most previous studies on TMD parameter optimization in galloping/flutter control have been limited in a linear framework, in which only the linear part of the aeroelastic force is considered. Accordingly, in galloping control of structures, some design formulas (Fujino and Abé 1993) have been derived to obtain the optimal stiffness and damping parameters that maximize the critical wind speed for a pre-selected TMD mass; in flutter control, the optimal stiffness and damping parameters for a pre-selected TMD mass should be determined through parametric analyses (Chen and Kareem 2003).

For a structure-TMD system with optimal stiffness and damping properties, both the effectiveness and robustness of the TMD can be enhanced by increasing the TMD mass (Fujino and Abé 1993; Chen and Kareem 2003). However, for a modern flexible, light-weighted structure, sometimes it might be necessary to make the TMD mass as low as possible due to some economical and practical considerations. To this end, it is of great significance to determine the minimum (and hence most economical) TMD mass that enables the aeroelastic system with sufficient wind-resistant capability, and then select an appropriate TMD mass according to some practical considerations (e.g., robustness and vibration amplitude of the TMD). Since the critical wind speed of a structure-TMD system with optimal stiffness and damping properties increases monotonically with increasing the TMD mass, it is convenient to obtain the minimum TMD mass that enables the conventional control target.

However, the conventional control target as well as the minimum TMD mass determined according to the aforementioned linear framework may be insufficient (and hence unsafe) because large-amplitude limit cycle oscillations (LCOs) or even divergent vibrations may occur (in cases with sufficiently large external excitations) well below the critical wind speed for some cross-sections due to the nonlinear aeroelastic effects (Novak 1972). On the other hand, it is known that the post-critical LCO amplitudes for some cross-sections (Zhang et al. 2017) grow very slowly with increasing the wind speed, resulting in relatively wide wind speed ranges with acceptable post-critical vibrations. As a result, the conventional control target and the minimum TMD mass determined according to the linear framework may be over-conservative (and hence uneconomical) since an occasional event of post-critical LCO with acceptable vibration amplitude is unlikely to result in significant fatigue damage or catastrophic failure to a modern structure. Consequently, it might be necessary to consider the nonlinear aeroelastic effect in order to determine the minimum TMD mass that enables the aeroelastic system with sufficient wind-resistant capability, and further select a more appropriate TMD mass in the galloping/flutter control according to some practical considerations. Casalotti et al. (2014) attempted to control the post-flutter oscillations of suspension bridges by hysteretic tuned mass dampers, in which the nonlinear aeroelastic forces were considered by the quasi-steady theory. They showed that the hysteretic tuned mass dampers can effectively control the post-flutter responses by reducing the LCO amplitudes to very low levels. They proposed that the flutter condition may be considered as a limit state with an acceptable vibration amplitude exhibited by the structure.

Following the idea of Casalotti et al. (2014), the present paper attempts to facilitate the control target with an acceptable vibration amplitude, i.e., to ensure that the vibration amplitude is lower than a threshold value before a target wind speed, which is referred to as the nonlinear control target in the following. To obtain the most economical TMD parameters that enable the nonlinear control target, an optimization procedure of TMD parameters involving nonlinear aeroelastic effect is developed for galloping control based on the quasi-steady aeroelastic force model, and for flutter control based on a nonlinear unsteady model. The optimization procedure is designed to determine the minimum TMD mass that enables the nonlinear target. The optimal frequency ratio and damping ratio are calculated based on existing formulations. Three numerical examples involving the galloping/flutter control of different cross-sections are analyzed to demonstrate the different results designed by the conventional and nonlinear targets.

## 2. A control target involving nonlinear aeroelastic effect

Two typical curves of self-excited LCO amplitude $q$ versus wind speed $U$ are schematically shown in Fig. 1(a) and Fig. 1(b), respectively, in which the critical wind speed $U_{cr}$ is highlighted by a solid rectangular marker; the amplitudes of stable (s) and unstable (us) LCOs are represented by solid and dashed lines, respectively; sn represents the point of a saddle-node bifurcation (Strogatz 1994). It is worth mentioning that, in the absence of any disturbance, both stable and unstable LCOs are theoretically possible steady-state motions of a system; however, it is unable to observe an unstable LCO in wind tunnel tests since disturbances (e.g., free-stream turbulence) are inevitable. The system in Fig. 1(a) exhibits convergent vibrations for $U < U_{cr}$, and performs LCOs after the occurrence of a supercritical Hopf bifurcation (Strogatz, 1994) at $U_{cr}$. On the other hand, for the system in Fig. 1(b), stable LCOs can occur after the saddle-node bifurcation (which occurs before $U_{cr}$) although an external disturbance (which should be larger than the amplitude of the unstable LCO) is required to excite the stable LCO; after the occurrence of a subcritical Hopf bifurcation at $U_{cr}$, the system can perform LCOs in the absence of any external disturbance. These bifurcations have been well studied by Strogatz (1994) and Nayfeh and Balachandran (2008) and these two typical self-excited responses have been analyzed for different aeroelastic systems by several authors, e.g., Dowell (1995).

It is obvious that the uncontrolled structures (red lines) in Figs. 1(a) and 1(b) cannot satisfy the conventional control target (i.e., $U_{cr} \geq U_{target}$) and are definitely unsafe, while the green lines both enable the conventional control target. However, for a modern structure with relatively large post-critical safety redundancy, the green line in Fig. 1(a) may be over-conservative since an occasional event of post-critical LCO with acceptable vibration amplitude is unlikely to result in significant fatigue damage or catastrophic failure to the structure. On the other hand, the green line in Fig. 1(b) may be unsafe because large-amplitude LCOs (or in other cases, divergent vibrations) can occur well before $U_{cr}$. As a result, concerning the galloping/flutter control of a structure with TMDs, the TMD parameters designed according to the conventional control target may be over-conservative or unsafe, depending on the aeroelastic behavior of the specific structure.

To this end, a nonlinear control target is introduced herein following the idea of Casalotti et al. (2014), i.e., to ensure $q \leq q_{thres}$ for $U \leq U_{target}$, where $q_{thres} \geq 0$ is an amplitude threshold pre-specified according to the expected structural performance. For a structure with relatively large post-critical safety redundancy, the nonlinear control target can take into account the post-critical safety redundancy of the structure by setting $q_{thres}$ as a positive value (i.e., the maximum allowable post-critical LCO amplitude), and hence result in a more economical design of TMDs. As an example, the blue line in Fig. 1(a) represents a design scheme that satisfies the nonlinear control target. It is noted that the slopes of various curves in Fig. 1(a) are not necessarily the same (indeed, a reduced slope is often desired for the controlled structure). Both the green line and blue line in Fig. 1(a) satisfy the nonlinear control target, while the blue line is obviously more economical (only considering the cost of the TMDs) than the green line.

On the other hand, for a structure that may experience large-amplitude LCO or divergent vibration before

$U_{cr}$, the nonlinear target can take into account the underlying large-amplitude vibrations before the critical state, and hence lead to more reliable design results of TMD parameters. If $q_{thres}$ = 0, the nonlinear control target is to completely mitigate the galloping/flutter vibrations below $U_{target}$. It is noted that the nonlinear control target with $q_{thres}$ = 0 is stricter than the conventional one (i.e., $U_{cr} \geq U_{target}$) because the former prohibits the occurrences of LCOs or divergent vibrations below $U_{target}$. As an example, the green line in Fig. 1(b) satisfies the conventional control target while it does not satisfy the nonlinear one; $U_{sn} \geq U_{target}$ (where $U_{sn}$ is the wind speed at the saddle-node point) is required to achieve the nonlinear control target, as demonstrated by the blue line in Fig. 1(b).

## 3. Optimization of TMD parameters involving nonlinear aeroelastic effect

In order to obtain the minimum (and hence most economical) TMD mass that enables the nonlinear control target, an optimization procedure of TMD parameters involving nonlinear aeroelastic effect is developed for galloping control based on the quasi-steady aeroelastic force model (Parkinson and Smith 1964), and for flutter control based on a nonlinear unsteady model (Zhang et al. 2019). The layouts of TMDs considered in the present work are schematically presented in Fig. 2 [the TMDs can be placed inside or outside the structure depending on the structure configuration, the two TMDs in Fig. 2(b) are identical], in which *B* and *D* represent the width and depth of the structural cross-section, respectively; $L_t$ is the distance between the centers of the structure and the TMDs. These layouts are commonly used in the control of wind-induced vibration of structures such as power transmission lines and bridges (e.g., Fujino and Abé 1993; Kwon and Park 2004), and the optimization procedures developed for the layouts in Figs. (2a) and (2b) are applicable for other structures with one and two degrees of freedom, respectively. It is noted that the spatial distribution of the wind along the span of the structure can change the critical condition and the post-critical responses (e.g., Arena et al. 2014). In this paper, it is assumed that the structure is exposed to a wind flow distributed uniformly along its span. In addition, the equations of motion in section 3.1 assumes that the vibration is dominated by a single mode, while the equations of motion in section 3.2 assumes that the vibration is dominated by a vertical mode and a torsional mode. These assumptions are widely adopted in the galloping and flutter analyses of line-like structures. However, these assumptions may lead to inaccurate results if the multimode coupling effect is significant (e.g., Chen and Kareem 2006; Arena and Lacarbonara 2012). An analysis considering the interaction of multiple modes is necessary for such a system.

### *3.1. Optimization of TMD parameters for galloping control based on quasi-steady theory*

According to the quasi-steady theory (Parkinson and Smith 1964), the governing equations for the galloping vibration of the structure-TMD system in Fig. 2(a) immersed in two-dimensional flow can be expressed as (Fujino and Abé 1993)

$$m_s(\ddot{y}_s + 2\xi_{s,y}\omega_{s,y}\dot{y}_s + \omega_s^2 y_s) = 0.5\rho U^2 D C_{Fy} + 2m_t\xi_t\omega_t(\dot{y}_t - \dot{y}_s) + m_t\omega_t^2(y_t - y_s) \quad (1a)$$

$$\ddot{y}_t + 2\xi_t\omega_t(\dot{y}_t - \dot{y}_s) + \omega_t^2(y_t - y_s) = 0 \quad (1b)$$

where $m_s$ and $m_t$ are the masses of the primary structure and TMD per unit length, respectively; $y_s$ and $y_t$ are the vertical displacements of the structure and TMD, respectively; overdot represents the derivative with respect to time $t$; $\xi_{s,y}$ and $\xi_t$ are the mechanical damping ratios of the structure and TMD, respectively; $\omega_{s,y}$ and $\omega_t$ represent the natural circular frequencies of the structure and TMD, respectively; $\rho$ is the air density; $D$ represents the depth of structural section; $U$ is the mean wind speed; $C_{Fy}$ represents the aeroelastic lift force coefficient which can be expanded as

$$C_{Fy} = \sum_{j=1}^{n} A_j \left(\frac{\dot{y}_s}{U}\right)^j \quad (2)$$

where $\frac{\dot{y}_s}{U} \approx \alpha$ is the effective angle of attack; $A_j$ ($j$ = 1 ~ $n$) are aeroelastic damping coefficients obtained through polynomial fitting on the experimental $C_{Fy}(\alpha)$ curve. For symmetric sections (with respect to the chord line), only odd-order terms are necessary for the polynomial expansion since even-order terms contribute insignificantly to the overall dynamics. For a section unsymmetrical with respect to the chord line (such as a bridge deck), even-order terms are also necessary (Arena et al. 2016). It is worth noting that the applicability of the quasi-steady theory should be limited to cases at relatively high reduced wind speeds without interference between galloping and vortex-induced vibration (Gao and Zhu 2017).

Introducing the dimensionless variables $\tau = \omega_{s,y} \cdot t$, $Y_s = y_s/D$, $Y_t = y_t/D$, and reduced wind speed $U_r = U/(\omega_{s,y} \cdot D)$, Eq. (1) can be expressed in the dimensionless form as

$$Y_s'' + 2\xi_{s,y} Y_s' + Y_s = \mu U_r^2 \sum_{j=0}^{n} A_j \left( \frac{Y_s'}{U_r} \right)^j + 2R_m R_f \xi_t \left( Y_t' - Y_s' \right) + R_m R_f^2 \left( Y_t - Y_s \right) \tag{3a}$$

$$Y_t'' + 2R_f \xi_t \left( Y_t' - Y_s' \right) + R_f^2 \left( Y_t - Y_s \right) = 0 \tag{3b}$$

where prime represents the derivative with respect to $\tau$; $\mu = \rho D^2/(2m_s)$; $R_m = m_t/m_s$ and $R_f = \omega_t/\omega_{s,y}$ are the mass ratio and frequency ratio between the TMD and the primary structure, respectively.

For a wide domain of engineering structures, it's known that the aeroelastic galloping force [of order $\mu U_r$ as shown in Eq. (3)] and mechanical damping force (of order $2\xi_{s,y}$) are small compared with the inertia force and mechanical stiffness force (both of order 1). The solutions of the governing equations tend to quasi-harmonic vibrations governed by the fundamental frequency components. This behavior is quite common for civil structures immersed in wind flow, where $\mu$ is typically of order $10^{-3}$. Accordingly, some asymptotic techniques, e.g., the averaging method (Nayfeh and Balachandran 2008), can be utilized to obtain the equivalent linearization approximation of the governing equations for the structure-TMD system. By assuming that the vibrations of the structure-TMD system are quasi-harmonic vibrations dominated by a single fast frequency, the aeroelastic damping expressed by the polynomial in Eq. (3a) can be approximated by an equivalent aeroelastic damping coefficient according to the averaging method

$$\begin{aligned} A_{1,eq}(q_s/U_r) &= -\frac{1}{\pi \cdot (q_s/U_r)} \int_0^{2\pi} \sum_{j=0}^{n} A_j \left( \frac{Y_s'}{U_r} \right)^j \sin\tau d\tau \\ &= \sum_{j=1}^{2n+1} 2A_j \frac{j!!}{(j+1)!!} (q_s/U_r)^{j-1} \end{aligned} \tag{4}$$

where !! represents the double factorial operation.

By replacing the aeroelastic damping coefficients $A_j$ ($j = 1 \sim n$) with the equivalent aeroelastic damping coefficient $A_{1,\,eq}(q_s/U_r)$, the equivalent linearization approximation of Eq. (3) can be obtained as

$$Y_s'' + 2\xi_{s,\,y} Y_s' - \mu U_r^2 A_{1,\,eq}(q_s/U_r)\frac{Y_s'}{U_r} + Y_s = 2R_m R_f \xi_t \left(Y_t' - Y_s'\right) + R_m R_f^2 \left(Y_t - Y_s\right) \tag{5a}$$

$$Y_t'' + 2R_f \xi_t \left(Y_t' - Y_s'\right) + R_f^2 \left(Y_t - Y_s\right) = 0 \tag{5b}$$

Eq. (5) can be expressed into the state-space format as

$$\begin{bmatrix} Y_s' \\ Y_t' \\ Y_s'' \\ Y_t'' \end{bmatrix} = \begin{bmatrix} 0 & 0 & 1 & 0 \\ 0 & 0 & 0 & 1 \\ -(1+R_m R_f^2) & R_m R_f^2 & -[2\xi_{s,\,y} + 2R_m R_f \xi_t - \mu U_r A_{1,\,eq}(q_s/U_r)] & 2R_m R_f \xi_t \\ R_f^2 & -R_f^2 & 2R_f \xi_t & -2R_f \xi_t \end{bmatrix} \cdot \begin{bmatrix} Y_s \\ Y_t \\ Y_s' \\ Y_t' \end{bmatrix} \tag{6}$$

It is noted that Eq. (6) is similar to the linear state-space equation utilized for TMD parameter optimization in Fujino and Abé (1993) except that $A_1$ in the linear equation is replaced by $A_{1,\,eq}(q_s/U_r)$ in Eq. (6). The eigenvalues of the structure-TMD system can be obtained through a complex eigenvalue analysis based on Eq. (6). The two pairs of complex eigenvalues, i.e., $\lambda_1$, $\lambda_1^*$, $\lambda_2$, $\lambda_2^*$ (where $*$ represents the complex conjugate), are related to the modal frequencies and damping ratios of the structure-TMD system as

$$\lambda_j = \omega_j \xi_j + i\omega_j \sqrt{1-\xi_j^2} \tag{7}$$

where $i = \sqrt{-1}$; $\omega_j$ and $\xi_j$ ($j$ = 1 or 2) are the modal circular frequencies and damping ratios corresponding to $\lambda_j$, respectively.

By substituting a specific $q_s/U_r$ (e.g., $q_s/U_r = a$) into Eq. (6), the eigenvalues of the structure-TMD system with pre-determined TMD parameters at various $U_r$ can be obtained through complex eigenvalue analyses, and an equivalent critical state is achieved when at least one of the modal damping ratios become zero. The equivalent critical state can be interpreted as an $U_r$ at which the LCO amplitude achieves $q_s = aU_r$. In the following part, the equivalent critical state will be denoted as $U_r(a)$ to avoid confusion with the linear critical state, i.e., $U_{r,\,cr} = U_r(0)$. For a given $R_m$, the optimal $R_f$ and $\xi_t$ that maximize the $U_r(a)$ can be determined by the formulas given in Fujino and Abé (1993), i.e.,

$$R_f = \frac{1}{\sqrt{1+R_m}} \quad (8a)$$

$$\xi_t = \sqrt{\frac{\sqrt{1+R_m}-1}{2\sqrt{1+R_m}}} \quad (8b)$$

In the present work, the purpose of TMD parameter optimization is to find a group of $R_f$, $\xi_t$, and $R_m$ that enables the nonlinear control target with the minimum $R_m$. Since the optimal $R_f$ and $\xi_t$ for a TMD with a specific $R_m$ are always determined by Eq. (8), the optimization purpose reduces to obtain the minimum $R_m$ that enables the nonlinear control target. For an aeroelastic system that exhibits a supercritical Hopf bifurcation at the critical wind speed [e.g., Fig. 1(a)], it is obvious that the nonlinear control target can be achieved if $U_r(q_{s,\ thres}/U_{r,\ target}) \geq U_{r,\ target}$. For an aeroelastic system that exhibits a subcritical Hopf bifurcation [e.g., Fig. 1(b)], if $q_{s,\ thres} \geq q_{s,\ sn}$, then $U_r(q_{s,\ thres}/U_{r,\ target}) \geq U_{r,\ target}$ also enables the nonlinear control target; however, if $q_{s,\ thres} \leq q_{s,\ sn}$, it is necessary to ensure $U_r(q_{s,\ sn}/U_{r,\ sn}) \geq U_{r,\ target}$ in order to achieve the nonlinear control target. The following procedure is then suggested for optimizing the TMD parameters (including $R_f$, $\xi_t$, and $R_m$) in galloping control:

(i) For the concerned structure, define an appropriate control target (i.e., $q_s \leq q_{s,\ thres}$ for $U_r \leq U_{r,\ target}$) according to the expected structural performance;

(ii) Calculate the galloping responses of the uncontrolled structure at various $U_r$ according to the quasi-steady aeroelastic force model;

(iii) Calculate the $A_{1,\ eq}(q_s/U_r)$ curve according to Eq. (4);

(iv) For a case that exhibits a supercritical Hopf bifurcation, substitute $A_{1,\ eq}(q_{s,\ thres}/U_{r,\ target})$ into Eq. (6), and obtain the equivalent critical state $U_r(q_{s,\ thres}/U_{r,\ target})$ of the structure-TMD system for various $R_m$ [with $R_f$ and $\xi_t$ determined by Eq. (8)] through complex eigenvalue analyses;

(v) For a case that exhibits a subcritical Hopf bifurcation, if $q_{s,\ thres} \geq q_{s,\ sn}$, substitute $A_{1,\ eq}(q_{s,\ thres}/U_{r,\ target})$ into Eq. (6), and obtain $U_r(q_{s,\ thres}/U_{r,\ target})$ of the structure-TMD system for various $R_m$ [with $R_f$ and $\xi_t$ determined by Eq. (8)] through complex eigenvalue analyses; if $q_{s,\,thres} \le q_{s,\,sn}$, substitute $A_{1,\,eq}(q_{s,\,sn}/U_{r,\,sn})$ into Eq. (6), and obtain $U_r(q_{s,\,sn}/U_{r,\,sn})$ of the structure-TMD system for various $R_m$ [with $R_f$ and $\xi_t$ determined by Eq. (8)] through complex eigenvalue analyses;

(vi) Determine the minimum $R_m$ that enables the control target according to the $U_r(q_{s,\,thres}/U_{r,\,target})$ versus $R_m$ curve [or $U_r(q_{s,\,sn}/U_{r,\,sn})$ versus $R_m$ curve if $q_{s,\,thres} \le q_{s,\,sn}$ for a case that exhibits a subcritical Hopf bifurcation]; the corresponding optimal $R_f$ and $\xi_t$ are determined by Eq. (8).

### *3.2. Optimization of TMD parameters for flutter control based on nonlinear unsteady theory*

The governing equations for the nonlinear flutter of the structure-TMD system in Fig. 2(b) immersed in two-dimensional flow can be expressed as (Gu et al. 1998)

$$m_s(\ddot{y}_s + 2\xi_{s,\,y}\omega_{s,\,y}\dot{y}_s + \omega_{s,\,y}^2 y_s) = F_{se} + m_t\xi_t\omega_t(\dot{y}_{t,\,1} - \dot{y}_s + \dot{y}_{t,\,2} - \dot{y}_s) + m_t\omega_t^2(y_{t,\,1} - y_s + y_{t,\,2} - y_s)/2 \tag{9a}$$

$$\begin{aligned} I_s(\ddot{\alpha}_s + 2\omega_{s,\,\alpha}\xi_{s,\,\alpha}\dot{\alpha}_s + \omega_{s,\,\alpha}^2\alpha_s) = M_{se} &- m_t L_t\xi_t\omega_t[(\dot{y}_{t,\,1} - \dot{y}_s + L_t\dot{\alpha}_s) - (\dot{y}_{t,\,2} - \dot{y}_s - L_t\dot{\alpha}_s)] \\ &- m_t L_t\omega_t^2[(y_{t,\,1} - y_s + L_t\alpha_s) - (y_{t,\,2} - y_s - L_t\alpha_s)]/2 \end{aligned} \tag{9b}$$

$$\ddot{y}_{t,\,1} + 2\xi_t\omega_t(\dot{y}_{t,\,1} - \dot{y}_s + L_t\dot{\alpha}_s) + \omega_t^2(y_{t,\,1} - y_s + L_t\alpha_s) = 0 \tag{9c}$$

$$\ddot{y}_{t,\,2} + 2\xi_t\omega_t(\dot{y}_{t,\,2} - \dot{y}_s - L_t\dot{\alpha}_s) + \omega_t^2(y_{t,\,2} - y_s - L_t\alpha_s) = 0 \tag{9d}$$

where $m_s$ and $I_s$ are the mass and mass inertia of the primary structure per unit length, respectively; $y_s$ and $\alpha_s$ are the vertical and torsional displacements of the structure, respectively; $\xi_{s,\,y}$ and $\xi_{s,\,\alpha}$ are the vertical and torsional mechanical damping ratios of the structure, respectively; $\omega_{s,\,y}$ and $\omega_{s,\,\alpha}$ are the vertical and torsional natural circular frequencies of the structure, respectively; $m_t = m_{t,\,1} + m_{t,\,2}$ is the total mass of two TMDs per unit length, with $m_{t,\,1}$ and $m_{t,\,2}$ representing the masses of the upstream and downstream TMD devices, respectively; in the present work, $m_{t,\,1} = m_{t,\,2}$; $y_{t,\,1}$ and $y_{t,\,2}$ are the vertical displacements of the upstream and downstream TMD devices, respectively; $F_{se}$ and $M_{se}$ are the self-excited lift force and torsional moment acting on the structure per unit length, respectively. In the present work, only $R_m = m_t/m_s$, $\omega_t$, and $\xi_t$ are considered as design parameters, while $L_t$ is assumed as a pre-determined value and $R_I = m_t L_t^2 / I_s$.

According to Zhang et al. (2019; 2020), $F_{se}$ and $M_{se}$ can be respectively expressed as

$$F_{se} = 0.5\rho U^2 B[KH_1^*(q_y/B,\ K)\frac{\dot{y}_s}{U} + KH_2^*(q_\alpha,\ K)\frac{\dot{\alpha}_s B}{U} + K^2 H_3^*(q_\alpha,\ K)\alpha_s + K^2 H_4^*(q_y/B,\ K)\frac{y_s}{B}] \tag{10a}$$

$$M_{se} = 0.5\rho U^2 B^2[KA_1^*(q_y/B,\ K)\frac{\dot{y}_s}{U} + KA_2^*(q_\alpha,\ K)\frac{\dot{\alpha}_s B}{U} + K^2 A_3^*(q_\alpha,\ K)\alpha_s + K^2 A_4^*(q_y/B,\ K)\frac{y_s}{B}] \tag{10b}$$

where $B$ represents the width of structural section; $K = \omega B/U$ is the reduced frequency; $q_y$ and $q_\alpha$ are the amplitudes of $y_s$ and $\alpha_s$, respectively; $H_i^*$ and $A_i^*$ ($i$ = 1 ~ 4) are nonlinear unsteady flutter derivatives with the amplitude-dependent feature.

By substituting Eq. (10) into Eq. (9), the equations of motion are actually linearized equations with amplitude-dependent aeroelastic damping and stiffness. For specific combinations of vertical and torsional vibration amplitudes, the linearized equations can be expressed in the state-space format with amplitude-dependent aeroelastic damping and stiffness as

$$\dot{\mathbf{Y}} = \mathbf{G}\mathbf{Y} \tag{11}$$

where **Y** is the state vector and **G** is the eigenvalue matrix, which can be respectively expressed as

$$\mathbf{Y} = [y_s \quad \alpha_s \quad y_{1,\,t} \quad y_{2,\,t} \quad \dot{y}_s \quad \dot{\alpha}_s \quad \dot{y}_{1,\,t} \quad \dot{y}_{2,\,t}]^{\mathrm{T}} \tag{12a}$$

$$\mathbf{G} = \begin{bmatrix} 0 & 0 & 0 & 0 & 1 & 0 & 0 & 0 \\ 0 & 0 & 0 & 0 & 0 & 1 & 0 & 0 \\ 0 & 0 & 0 & 0 & 0 & 0 & 1 & 0 \\ 0 & 0 & 0 & 0 & 0 & 0 & 0 & 1 \\ G_{5,\,1} & G_{5,\,2} & 0.5R_m\omega_t^2 & 0.5R_m\omega_t^2 & G_{5,\,5} & G_{5,\,6} & R_m\xi_t\omega_t & R_m\xi_t\omega_t \\ G_{6,\,1} & G_{6,\,2} & -m_tL_t\omega_t^2/(2I_s) & m_tL_t\omega_t^2/(2I_s) & G_{6,\,5} & G_{6,\,6} & -R_I\xi_t\omega_t/L_t & R_I\xi_t\omega_t/L_t \\ \omega_t^2 & -\omega_t^2L_t & -\omega_t^2 & 0 & 2\xi_t\omega_t & -2\xi_t\omega_tL_t & -2\xi_t\omega_t & 0 \\ \omega_t^2 & \omega_t^2L_t & 0 & -\omega_t^2 & 2\xi_t\omega_t & 2\xi_t\omega_tL_t & 0 & -2\xi_t\omega_t \end{bmatrix} \tag{12b}$$

where $G_{5,\,1}$, $G_{5,\,2}$, $G_{5,\,5}$, $G_{5,\,6}$, $G_{6,\,1}$, $G_{6,\,2}$, $G_{6,\,5}$, and $G_{6,\,6}$ can be respectively expressed as

$$G_{5,\,1} = -\omega_{s,\,y}^2 - R_m\omega_t^2 + 0.5\rho U^2K^2H_4^*(q_y/B,\ K) \tag{13a}$$

$$G_{5,\,2} = 0.5\rho U^2BK^2H_3^*(q_\alpha,\ K) \tag{13b}$$

$$G_{5,\,5} = -2\xi_{s,\,y}\omega_{s,\,y} - 2R_m\xi_t\omega_t + 0.5\rho UBKH_1^*(q_y/B,\ K) \tag{13c}$$

$$G_{5,\,6} = 0.5\rho UB^2KH_2^*(q_\alpha,\ K) \tag{13d}$$

$$G_{6,\,1} = 0.5\rho U^2BK^2A_4^*(q_y/B,\ K) \tag{13e}$$

$$G_{6,\,2} = -\omega_{s,\,\alpha}^{2} - R_I \omega_t^2 + 0.5\rho U^2 B^2 K^2 A_3^*(q_\alpha,\, K) \quad (13f)$$

$$G_{6,\,5} = 0.5\rho U B^2 K A_1^*(q_y / B,\, K) \quad (13g)$$

$$G_{6,\,6} = -2\xi_{s,\,\alpha}\omega_{s,\,\alpha} - 2R_I \xi_t \omega_t + 0.5\rho U B^3 K A_2^*(q_\alpha,\, K) \quad (13h)$$

It is noted that Eq. (11) is similar to the linear state-space equation utilized for TMD parameter optimization in Gu et al. (1998) except that the flutter derivatives in Eq. (11) are dependent on vibration amplitudes. By substituting the flutter derivatives at specific vertical and torsional vibration amplitudes into Eq. (11), the eigenvalues of the structure-TMD system with pre-determined TMD parameters at various $U$ can be obtained through complex eigenvalue analyses, and an equivalent critical state is achieved when at least one of the modal damping ratios become zero. The equivalent critical state can be interpreted as a wind speed at which one or both of the (vertical and torsional) vibration amplitudes achieve the pre-specified values. In the following part, the equivalent critical state will be denoted as $U(q_y,\ q_\alpha)$, $U(q_y)$, or $U(q_\alpha)$, depending on which amplitude(s) achieve the pre-specified value(s). It should be stated that, for a specific $R_m$, parametric analyses are required to obtain the optimal $\omega_t$ and $\xi_t$ since analytical formulas are unavailable.

For an aeroelastic system that may encounter vertical-torsional coupled flutter, the nonlinear control target can be set as $q_y \le q_{y,\, thres}$ and $q_\alpha \le q_{\alpha,\, thres}$ for $U \le U_{target}$, where $q_{y,\, thres}$ and $q_{\alpha,\, thres}$ are vertical and torsional amplitude thresholds pre-specified according to the expected structural performance, respectively. Similar to the procedure for galloping control, an optimization procedure for flutter control is presented as follows:

(i) For the concerned structure, define an appropriate control target (i.e., $q_y \le q_{y,\, thres}$ and $q_\alpha \le q_{\alpha,\, thres}$ for $U \le U_{target}$) according to the expected structural performance;

(ii) Calculate the nonlinear flutter responses of the uncontrolled structure at various $U$ according to the nonlinear unsteady aeroelastic force model;

(iii) For a case that exhibits a supercritical Hopf bifurcation, substitute the flutter derivatives at $q_y = q_{y,\, thres}$ and $q_\alpha = q_{\alpha,\, thres}$ into Eq. (11), and obtain the equivalent critical state [i.e., $U(q_{y,\, thres},\ q_{\alpha,\, thres})$, $U(q_{y,\, thre})$, or $U(q_{\alpha,$

$_{thre}$)] of the structure-TMD system for various $R_m$ (with corresponding optimal $\omega_t$ and $\xi_t$ determined through parametric analyses) through complex eigenvalue analyses;

(iv) For a case that exhibits a subcritical Hopf bifurcation, if $q_{y, thres} \geq q_{y, sn}$ and $q_{\alpha, thres} \geq q_{\alpha, sn}$, substitute the flutter derivatives at $q_y \leq q_{y, thres}$ and $q_\alpha \leq q_{\alpha, thres}$ into Eq. (11), and obtain the equivalent critical states [i.e., $U(q_y, q_\alpha)$, $U(q_y)$, or $U(q_\alpha)$] of the structure-TMD system with flutter derivatives at various vibration states for various $R_m$ (with corresponding optimal $\omega_t$ and $\xi_t$ determined through parametric analyses) through complex eigenvalue analyses; if $q_{y, thres} \leq q_{y, sn}$ or $q_{\alpha, thres} \leq q_{\alpha, sn}$, substitute the flutter derivatives at $q_y \leq q_{y, sn}$ and $q_\alpha \leq q_{\alpha, sn}$ into Eq. (11) and obtain the equivalent critical states of the structure-TMD system with flutter derivatives at various vibration states for various $R_m$ (with corresponding optimal $\omega_t$ and $\xi_t$ determined through parametric analyses) through complex eigenvalue analyses;

(v) For a case that exhibits a supercritical Hopf bifurcation, determine the minimum $R_m$ that enables the control target according to the curve of equivalent critical state [i.e., $U(q_{y, thres}, q_{\alpha, thres})$, $U(q_{y, thre})$, or $U(q_{\alpha, thre})$] versus $R_m$; for a case that exhibits a subcritical Hopf bifurcation, determine the values of $R_m$ at various vibration states according to the curves of equivalent critical states [i.e., $U(q_y, q_\alpha)$, $U(q_y)$, or $U(q_\alpha)$] versus $R_m$, and the largest value at various vibration states is the minimum $R_m$ that enables the nonlinear control target; the corresponding optimal $\omega_t$ and $\xi_t$ can be determined through parametric analyses.

It is noted that the difference between the design results of the new optimization procedure and the conventional one is essentially due to their different control targets, and the difference is determined by the considered structure and design targets. For the differences between the results of the two targets, the main parameter of interest is the TMD mass. The purpose of the new optimization procedure is to determine the minimum TMD mass that enables the nonlinear control target. In practical applications, a larger value may be required to improve the effectiveness and robustness of the TMDs. Moreover, it should be stated that the vibration amplitude of a TMD device increases with decreasing its mass, which may limit the practical application of a TMD device with a very small mass. Therefore, the space constraint for the TMD installation might be another important parameter to consider in practical applications.

# 4. Numerical examples

## *4.1. Galloping control*

The galloping controls for two cross-sections are studied in this subsection to demonstrate the different results designed by the conventional and nonlinear targets. The two selected cross-sections are representatives of structures that exhibit the typical galloping responses shown in Figs. 1(a) and 1(b), respectively. Throughout this subsection, $\mu$ = 1/1000 and $\xi_{s,y}$ = 3.0‰ for both cross-sections. It should be stated that the optimization purpose in the following analyses is to determine the minimum TMD mass that enables the expected control target, while the applicability and robustness of the minimum TMD mass are not analyzed. The bifurcation diagram of a structure-TMD system is generated using the following procedure. By substituting the $A_{1,eq}(q_s/U_r)$ at a specific value of $q_s/U_r$ into the state-space equation of motion, i.e., Eq. (6), the eigenvalues of the structure-TMD system with pre-determined TMD parameters at various reduced wind speeds can be obtained through complex eigenvalue analyses. An equivalent critical state is achieved when at least one of the modal damping ratios of the coupled system becomes zero. The equivalent critical state can be interpreted as a limit state of the structure-TMD system. More specifically, the critical state can be interpreted as follows: the structure can perform limit cycle oscillation with an amplitude of $q_s$ at a reduced wind speed of $U_r$. The stability of the limit state oscillation is then examined by numerical time integration of the equations of motion [i.e., Eq. (3) or (5)] using the 4$^{th}$-order Runge-Kutta method. The bifurcation diagram can be generated when the critical states corresponding to various values of $q_s/U_r$ are available.

**Case A: galloping of a simulated system exhibits a supercritical Hopf bifurcation**

The galloping control for a simulated aeroelastic system with $A_1$ = 8.0, $A_3$ = −150.0, and $A_j$ = 0 ($j \neq$ 1 or 3) is investigated as the first example. The $C_{Fy}(\alpha)$ and $A_{1,eq}(q_s/U_r)$ curves of the simulated system are shown in Figs. 3(a) and 3(b), respectively. The galloping response of the uncontrolled structure is presented in Fig. 4(a), in which the linear critical state is highlighted by a solid rectangular marker.

The structure analyzed in this example is supposed to be one with relatively large post-critical safety redundancy, and the target reduced wind speed for galloping control is supposed as $U_{r,target} = 20$. Accordingly, the nonlinear control target is to ensure that $q_s \leq q_{s,thres} = 2$ for $U_r \leq U_{r,target} = 20$. The conventional one reduces to ensure that $U_{r,cr} \geq U_{r,target} = 20$ since it focuses on $U_{r,cr}$.

The conventional optimization procedure is firstly utilized to determine the minimum $R_m$ that enables the conventional control target. The $U_{r,cr}$ of the structure-TMD system for various $R_m$ [with $R_f$ and $\xi_t$ determined by Eq. (8)] are obtained through complex eigenvalue analyses based on Eq. (6), and the results are shown in Fig. 5. The results suggest that a TMD with $R_m = 2.5\%$ is able to enable $U_{r,cr} \geq U_{r,target} = 20$. The steady-state $q_s$ and $q_t$ (steady-state amplitude of $Y_t$) of the structure-TMD system with $R_m = 2.5\%$ are shown in Fig. 4. It is noted that galloping vibrations are completely mitigated for $U_r \leq U_{r,target} = 20$ as expected. However, $R_m = 2.5\%$ should be over-conservative for this specific case considering its post-critical safety redundancy.

The new optimization procedure is then utilized to determine the minimum $R_m$ that enables the nonlinear control target. As noticed from Fig. 3(b), $q_{s,thres}/U_{r,target} = 2/20$ corresponds to an $A_{1,eq}(2/20) \approx 6.88$. $A_{1,eq}(2/20) = 6.88$ is then substituted into Eq. (6), and the $U_r(q_{s,thres}/U_{r,target})$ of the structure-TMD system for various $R_m$ [with $R_f$ and $\xi_t$ determined by Eq. (8)] are obtained through complex eigenvalue analyses, as shown in Fig. 5. The results suggest that a TMD with $R_m = 1.8\%$ is sufficient to ensure $q_s \leq q_{s,thres} = 2$ for $U_r \leq U_{r,target} = 20$. The steady-state $q_s$ and $q_t$ of the structure-TMD system with $R_m = 1.8\%$ shown in Fig. 4 further demonstrate that $R_m = 1.8\%$ determined by the proposed optimization procedure is the minimum (and hence most economical) value that enables the nonlinear control target. This example suggests that the nonlinear control target and optimization procedure are more economical than the conventional ones in designing TMDs for galloping control of a modern structure with relatively large post-critical safety redundancy.

**Case B: galloping of a *B*/*D* = 2 rectangular section**

The second example analyzes the galloping control for a $B/D$ = 2 rectangular section. The $C_{Fy}(\alpha)$ [constructed from the experimental measurements in Santosham (1966)] and $A_{1,\ eq}(q_s/U_r)$ curves for this cross-section are shown in Figs. 6(a) and 6(b), respectively. The aeroelastic damping coefficients are $A_1$ = 2.33, $A_3 = 1.10 \times 10^3$, $A_5 = -7.42 \times 10^4$, $A_7 = 1.66 \times 10^6$, $A_9 = -1.61 \times 10^7$, $A_{11}$ = 5.73, and $A_j = 0$ ($j \neq 1$, 3, 5, 7, 9, or 11). The galloping response of the uncontrolled structure is presented in Fig. 7(a), in which hysteresis phenomenon is observed around $U_r = 1 \sim 2.5$.

For this example, it is expected that no galloping vibrations can occur below $U_{r,\ target}$ = 25 regardless of the initial excitation. Accordingly, the nonlinear control target is to completely mitigate the galloping vibrations below $U_{r,\ target}$ = 25. The conventional one reduces to ensure that $U_{r,\ cr} \geq U_{r,\ target}$ = 25 since it focuses on $U_{r,\ cr}$.

The $U_{r,\ cr}$ of the structure-TMD system for various $R_m$ [with $R_f$ and $\xi_t$ determined by Eq. (8)] are obtained through complex eigenvalue analyses based on Eq. (6), as presented in Fig. 8. The results suggest that a TMD with $R_m$ = 0.3% can ensure the linear stability (i.e., the stability of the equilibrium position) of the structure-TMD system below $U_{r,\ target}$, i.e, $U_{r,\ cr} > U_{r,\ target}$ = 25, while it is unable to shed light on the underlying LCO control before $U_{r,\ cr}$. The steady-state $q_s$ and $q_t$ of the structure-TMD with $R_m$ = 0.3% and corresponding optimal $R_f$ and $\xi_t$ are shown in Figs. 7. It is noted that $U_{r,\ cr} > U_{r,\ target}$ = 25 as expected, while LCOs with relatively large amplitudes occur well before $U_{r,\ target}$ = 25. The results suggest that the conventional control target and optimization procedure in the linear framework may lead to unsafe design results of TMD parameters in the galloping control for similar cross-sections.

To completely mitigate the galloping vibrations below $U_{r,\ target}$ = 25, $A_{1,\ eq}(q_{s,\ sn}/U_{r,\ sn})$ = 7.01 should be utilized in the optimization procedure. The $U_r(q_{s,\,sn}/U_{r,\,sn})$ of the structure-TMD system are obtained for various $R_m$ [with $R_f$ and $\xi_t$ determined by Eq. (8)] though complex eigenvalue analyses based on Eq. (6), as shown in Fig. 8. The results suggest that a TMD with $R_m$ = 3.0% should be adopted to enable the nonlinear control target. The steady-state $q_s$ and $q_t$ of the structure-TMD system with $R_m$ = 3.0% and corresponding optimal $R_f$ and $\xi_t$ presented in Figs. 7 further demonstrate that $R_m$ = 3.0% is the minimum $R_m$ that enables the nonlinear control target. Note that $R_m$ = 3.0% is much higher than $R_m$ = 0.3% obtained using the conventional procedure. This example demonstrates that the nonlinear control target and optimization procedure are capable of controlling the underlying LCOs before the critical galloping wind speed, and hence they are more reliable than the conventional ones in designing the TMD parameters for galloping control of structures.

### *4.2. Flutter control*

The flutter control of a $B/D$ = 13 rectangular section is studied in this subsection. It is noted that the vibration frequency of an aeroelastic system may vary continuously with increasing the wind speed due to the aeroelastic stiffness effect, and hence multiple TMDs with distributed frequencies are often utilized in flutter control to enhance the robustness at various wind speeds (Kwon and Park 2004). However, since the main purpose of the present work is to highlight the effect of the nonlinear aeroelastic force, only two TMDs with identical parameters are considered. In addition, only $R_m$, $\omega_t$, and $\xi_t$ are considered as design parameters, while $L_t$ is assumed as a pre-determined value; to reduce the computational costs, $R_f$ (it is assumed that $\omega_t = R_f\omega_{cr}$, where $\omega_{cr}$ is the circular frequency at the critical wind speed of the uncontrolled structure) and $\xi_t$ for a specific $R_m$ is always obtained through Eq. (8) instead of a parametric analysis in the following analyses.

**Case C: vertical-torsional coupled flutter of a *B*/*D* = 13 rectangular section**

Flutter derivatives for the considered cross-section can be found in Noda et al. (2003). The flutter performance of this section is similar to some streamlined bridge decks and hence it is often studied as a simplified bridge deck section. Only the amplitude-dependency of $H_2^*$, $A_2^*$, and $A_3^*$ are considered in the present example since other flutter derivatives are almost independent of vibration amplitudes. It is noted that in practical flutter control of a long-span bridge, the geometric nonlinearity originating from the cables (e.g., Arena et al. 2012) should also be considered while the geometric nonlinearity is not considered in this paper. The modal parameters of this example are $m_s$ =3.0 × $10^4$ kg/m, $I_s$ =3.0 × $10^6$ kg·m$^2$/m, $\omega_{s,h}$ = 0.63 rad/s, $\omega_{s,\alpha}$= 1.51 rad/s, $\xi_{s,h}$ = 5.0‰, $\xi_{s,\alpha}$= 5.0‰, $B$ = 30 m, and $L_t$ = 13 m. According to a complex eigenvalue analysis with flutter derivatives at a small vibration amplitude (i.e., $q_\alpha$ = 1.3°), $U_{cr}$ = 57.8 m/s for the uncontrolled structure. However, due to the amplitude-dependency of some flutter derivatives, divergent vibrations may occur (in cases with sufficiently large external excitations) well below $U_{cr}$ = 57.8 m/s. As an example, the displacement responses of the uncontrolled structure at $U$ = 56.0 m/s starting from two different initial conditions are presented in Fig. 9(a), in which $q_0$ represents the initial vibration amplitude. Only the torsional displacements are given for brevity. It is noted that the uncontrolled structure performs divergent vibration at $U$ = 56.0 m/s (< $U_{cr}$ = 57.8 m/s) if the initial excitation is sufficiently large. For this example, the nonlinear control target is to completely mitigate the self-excited vibrations below $U_{target}$ = 62 m/s, while the conventional one is to ensure that $U_{cr} \geq U_{target}$ = 62 m/s.

By substituting the flutter derivatives at a small vibration amplitude (i.e., $q_\alpha$ = 1.3°) into Eq. (11), the $U_{cr}$ of the structure-TMD system for various $R_m$ [with $R_f$ and $\xi_t$ determined by Eq. (8)] are obtained through complex eigenvalue analyses, and the results are shown in Fig. 10. The results suggest that a TMD with $R_m$ = 0.56% can ensure $U_{cr} \geq U_{target}$ = 62 m/s, while it is unable to shed light on the control of the underlying divergent vibrations before $U_{cr}$. Fig. 9(b) presents the displacement responses of the structure-TMD system with $R_m$ = 0.56% at $U$ = 61.0 m/s starting from two different initial conditions. It is noted the controlled structure may be unsafe since divergent vibration can occur at $U$ = 61.0 m/s (< $U_{target}$ = 62 m/s) if the initial excitation is sufficiently large.

By substituting the flutter derivatives at all available vibration amplitudes into Eq. (11), the $U(q_\alpha)$ of the structure-TMD system for various $R_m$ [with $R_f$ and $\xi_t$ determined by Eq. (8)] are obtained through complex eigenvalue analyses, as presented in Fig. 10. The results suggest that a TMD with $R_m$ = 3.50% can be adopted to enable the nonlinear control target. Fig. 9(c) presents the displacement responses of the structure-TMD system with $R_m$ = 3.50% at $U_{target}$ = 62 m/s starting from two different initial conditions. It is noted that the structure always performs convergent vibrations, and hence the nonlinear control target is achieved. This example demonstrates that the nonlinear control target and optimization procedure are capable of controlling the underlying divergent vibrations before the linear critical state, and hence they are more reliable than the conventional ones in designing the TMD parameters for flutter control of structures.

It should be mentioned that that TMDs are not suitable for the flutter control of a bridge deck if its negative aeroelastic damping varies rapidly with wind speed beyond the critical value (Chen and Kareem 2003). For such a bridge deck, a very large additional damping ratio is required to increase its critical flutter wind speed. Therefore, both the conventional and nonlinear targets will result in a very large mass ratio since the effective damping ratio provided by the TMDs is proportional to the mass ratio.

## 5. Conclusions

The present paper discusses some shortcomings of the conventional target for self-excited galloping/flutter control and further introduces a nonlinear target, i.e., to ensure that the vibration amplitude is lower than a threshold value (pre-specified according to the expected structural performance) before a target wind speed. An optimization procedure of TMD parameters involving nonlinear aeroelastic effect is accordingly developed in order to determine the minimum TMD mass that enables the nonlinear target.

Three numerical examples involving the galloping/flutter control of different cross-sections are analyzed to demonstrate the different results designed by the conventional and nonlinear targets. Results of the numerical examples demonstrate that: for a structure with relatively large post-critical safety redundancy, the nonlinear target can take into account the post-critical safety redundancy and hence lead to more economical design results; for a structure that may experience large-amplitude vibrations before the critical wind speed, the nonlinear target is more reliable since it can shed light on the control of LCOs or divergent vibrations before the critical state. The nonlinear control target and proposed optimization procedure may be utilized in the optimization of TMD parameters for self-excited galloping/flutter control of structures in a wide domain of engineering fields.

## CRediT authorship contribution statement

**Mingjie Zhang:** Methodology, Software, Formal analysis, Writing original draft. **Fuyou Xu:** Supervision, Conceptualization, Formal analysis, Writing original draft.

## Declaration of Competing Interest

The authors declare that they have no known competing financial interests or personal relationships that could have appeared to influence the work reported in this paper.


## Acknowledgement

This research is supported by the National Natural Science Foundation of China (51978130, 52125805).


## Appendix. List of symbols

$A_{1,eq}$ = equivalent aeroelastic damping coefficient

$A_j$ = aeroelastic damping coefficients

$B$ = width of cross-section

$C_{Fy}$ = aeroelastic lift force coefficient

$D$ = depth of cross-section

$H_i^*$, $A_i^*$ = flutter derivatives

$I_s$ = mass inertia of primary structure

$K$ = reduced frequency

$L_t$ = distance between centers of TMD and primary structure

$m_s$ = mass of primary structure

$m_t$ = mass of TMD

$q_s$ = dimensionless vertical amplitude of primary structure

$q_t$ = dimensionless vertical amplitude of TMD

$q_y$ = vertical amplitude of primary structure

$q_\alpha$ = torsional amplitude of primary structure

$q_{s,\,thres}$ = dimensionless vertical amplitude threshold

$q_{\alpha,\,thres}$ = torsional amplitude threshold

$R_f$ = frequency ratio between TMD and primary structure

$R_I$ = mass inertia ratio between TMD and primary structure

$R_m$ = mass ratio between TMD and primary structure

$t$ = time

$U$ = wind speed

$U_{cr}$ = critical wind speed

$U_r$ = reduced wind speed

$U_{r,\,cr}$ = critical reduced wind speed

$U_{r,\,target}$ = target reduced wind speed

$U_{target}$ = target wind speed

$Y_s$ = dimensionless vertical displacement of primary structure

$Y_t$ = dimensionless vertical displacement of TMD

$y_s$ = vertical displacement of primary structure

$y_t$ = vertical displacement of TMD

$\alpha \approx \frac{\dot{y}_s}{U}$ = effective angle of attack

$\alpha_s$ = torsional displacement of primary structure

$\omega_{s,\,y}$ = vertical natural circular frequency of primary structure

$\omega_{s,\,\alpha}$ = torsional natural circular frequency of primary structure

$\omega_t$ = natural circular frequency of TMD

$\xi_{s,\,y}$ = vertical mechanical damping ratio of primary structure

$\xi_{s,\,\alpha}$ = torsional mechanical damping ratio of primary structure

$\xi_t$ = damping ratio of TMD

$\rho$ = air density

$\mu = \rho D^2/(2m_s)$ = density ratio between fluid and structure

$\tau = \omega_s t$ = dimensionless time

## References


Arena, A., and Lacarbonara, W., 2012. "Nonlinear parametric modeling of suspension bridges under aeroelastic forces: torsional divergence and flutter. " Nonlinear Dynam. 70(4): 2487-2510.

Arena, A., Lacarbonara, W., and Marzocca, P., 2016. "Post-critical behavior of suspension bridges under nonlinear aerodynamic loading." J. Comput. Nonlin. Dyn. 11(1): 011005.

Arena, A., Lacarbonara, W., Valentine, D.T., and Marzocca, P., 2014. Aeroelastic behavior of long-span suspension bridges under arbitrary wind profiles. J. Fluids Struct. 50: 105-119.

Casalotti, A., Arena, A., and Lacarbonara, W., 2014. "Mitigation of post-flutter oscillations in suspension bridges by hysteretic tuned mass dampers." Eng. Struct. 69: 62-71.

CCCC Highway Consultants, 2004. Wind-resistant Design Specification for Highway Bridges. Beijing, China.

Chen, X., and Kareem, A. 2003. "Efficacy of tuned mass dampers for bridge flutter control." J. Struct. Eng. 129 (10): 1291-1300.

Chen, X., and Kareem, A., 2006. "Revisiting multimode coupled bridge flutter: some new insights." J. Eng. Mech. 132(10): 1115-1123.

Dowell, E.H. 1995. A Modern Course in Aeroelasticity. Kluwer, Dordrecht.

Fujino, Y., and Abé, M. 1993. "Design formulas for tuned mass dampers based on a perturbation technique." Earthq. Eng. Struct. D. 22 (10): 833-854.

Gao, G., and Zhu, L. 2017. "Nonlinear mathematical model of unsteady galloping force on a rectangular 2: 1 cylinder." J. Fluids Struct. 70: 47-71.

Gu, M., Chang, C. C., Wu, W., and Xiang, H. F. 1998. "Increase of critical flutter wind speed of long-span bridges using tuned mass dampers." J. Wind Eng. Ind. Aerodyn. 73 (2): 111-123.

Kwon, S.D., and Park, K.S. 2004. "Suppression of bridge flutter using tuned mass dampers based on robust performance design." J. Wind Eng. Ind. Aerodyn. 92 (11): 919-934.

Nayfeh, A.H. and Balachandran, B., 2008. Applied nonlinear dynamics: analytical, computational, and experimental methods. John Wiley & Sons.

Noda, M., Utsunomiy, H., Nagao, F., Kanda, M., and Shiraishi, N. 2003. "Effects of oscillation amplitude on aerodynamic derivatives." J. Wind Eng. Ind. Aerodyn. 91 (1-2): 101-111.

Novak, M. 1972. “Galloping oscillations of prismatic structures.” J. Eng. Mech. Div. 98: 27-46.

Parkinson, G. V., and Smith, J. D. 1964. “The square prism as an aeroelastic nonlinear oscillator.” Q. J. Mech. Appl. Math. 17: 225–239.

Santosham, T. V. 1966. *Force measurements on bluff cylinders and aeroelastic galloping of a rectangular cylinder*. Master thesis, University of British Columbia.

Strogatz, S. H. 1994. *Nonlinear dynamics and chaos: with applications to physics, biology, chemistry, and engineering*. New York: CRC Press.

Zhang, M., Xu, F. and Han, Y., 2020. “Assessment of wind-induced nonlinear post-critical performance of bridge decks.” J. Wind Eng. Ind. Aerodyn. 203: 104251.

Zhang, M., Xu, F., and Ying X. 2017. “Experimental investigations on the nonlinear torsional flutter of a bridge deck.” J. Bridge Eng. 22 (8): 04017048.

Zhang, M., Xu, F., Zhang, Z., and Ying X. 2019. “Energy budget analysis and engineering modeling of post-flutter limit cycle oscillation of a bridge deck.” J. Wind Eng. Ind. Aerodyn. 188: 410-420.

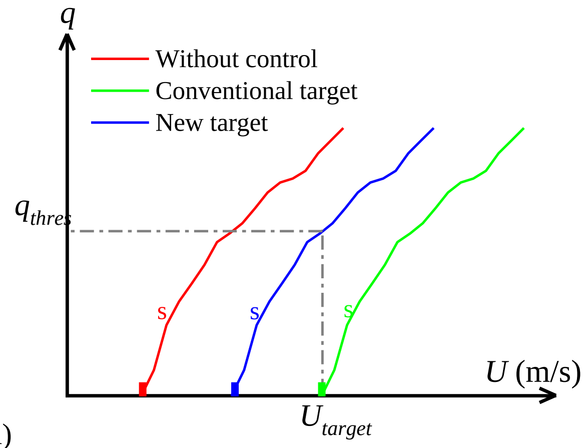


(a)

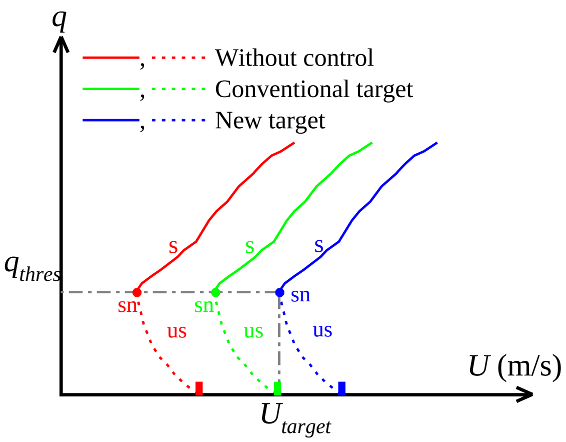


(b)

**Fig. 1.** Schematic diagrams of conventional and nonlinear control targets: (a) Supercritical Hopf bifurcation at $U_{cr}$; (b) Subcritical Hopf bifurcation at $U_{cr}$. Solid rectangular marker: $U_{cr}$; s: stable; us: unstable; sn: saddle node

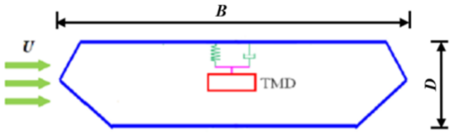


(a)

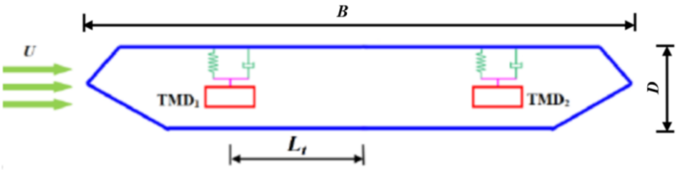


(b)

**Fig. 2.** Schematic diagrams of structure-TMD systems: (a) Layout of TMD for galloping control; (b) Layout of TMDs for flutter control

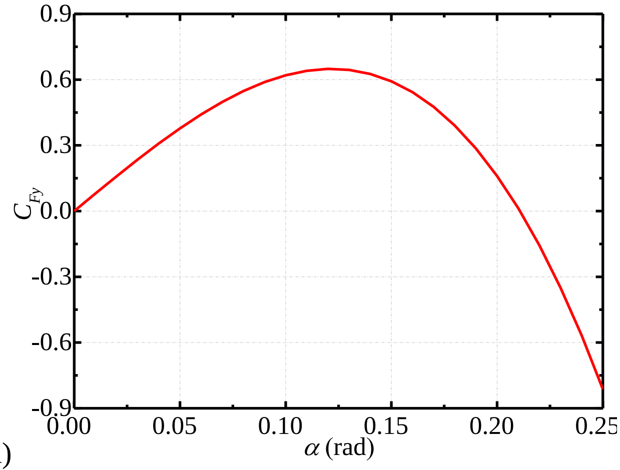


(a)

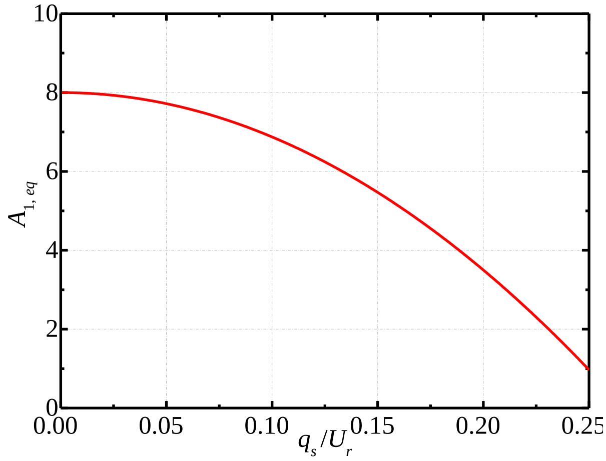


(b)

**Fig. 3.** Case A, aeroelastic parameters: (a) $C_{Fy}(\alpha)$; (b) $A_{1,\,eq}(q_s/U_r)$

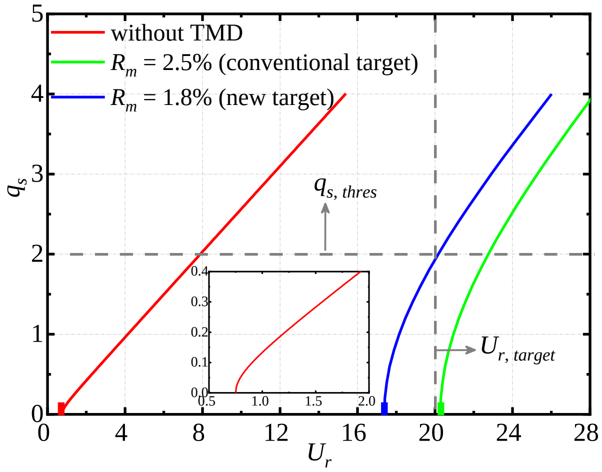


(a)

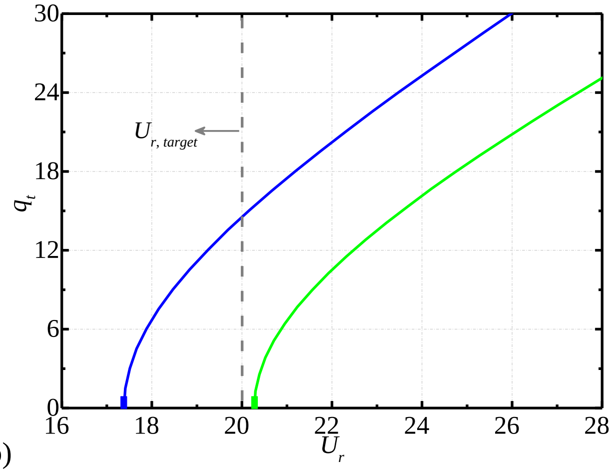


(b)

**Fig. 4.** Case A, galloping behaviors of uncontrolled structure and structure-TMD systems with $R_m$ = 2.5% and 1.8%: (a) $q_s$ versus $U_r$ ; (b) $q_t$ versus $U_r$

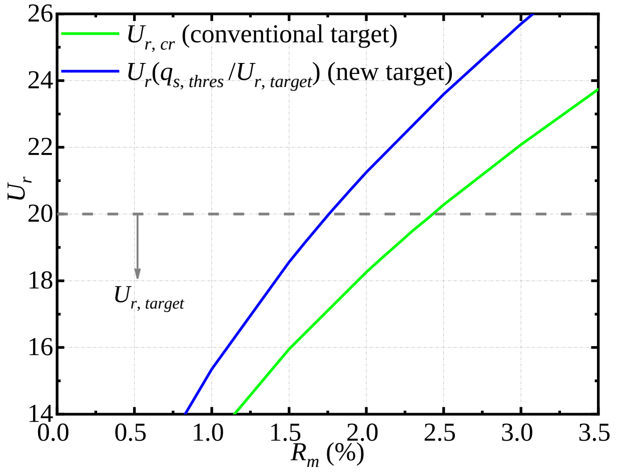


**Fig. 5.** Case A, $U_{r,\,cr}$ and $U_r(q_{s,\,target}/U_{r,\,target})$ versus $R_m$

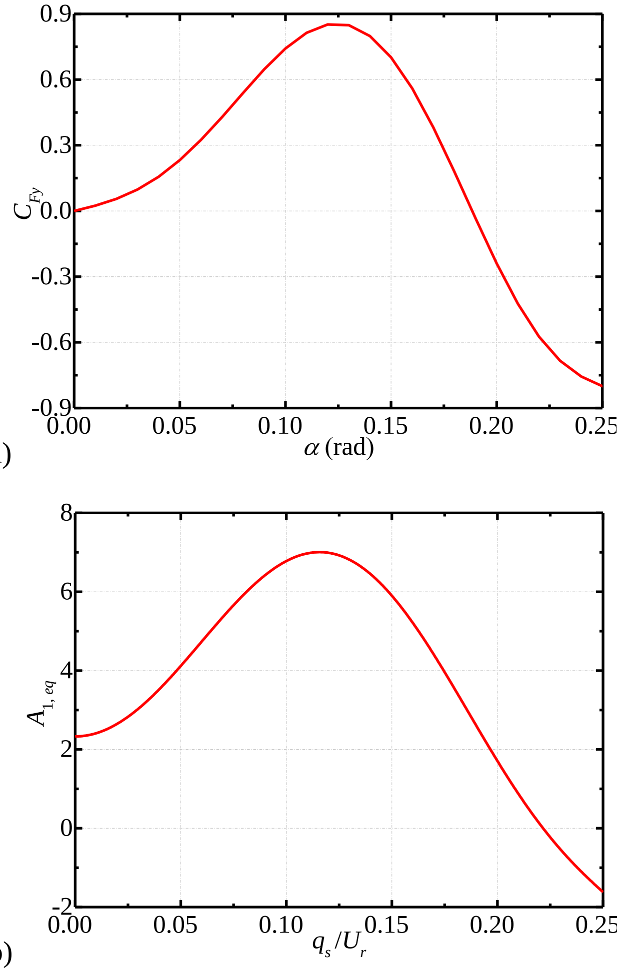


(a)

(b)

**Fig. 6.** Case B, aeroelastic parameters: (a) $C_{Fy}(\alpha)$; (b) $A_{1,\,eq}(q_s/U_r)$

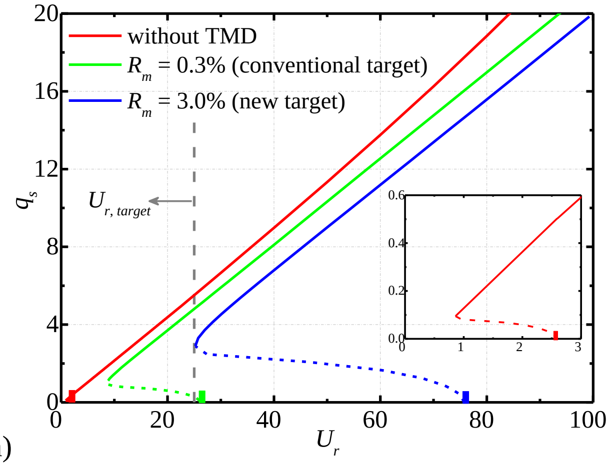


(a)

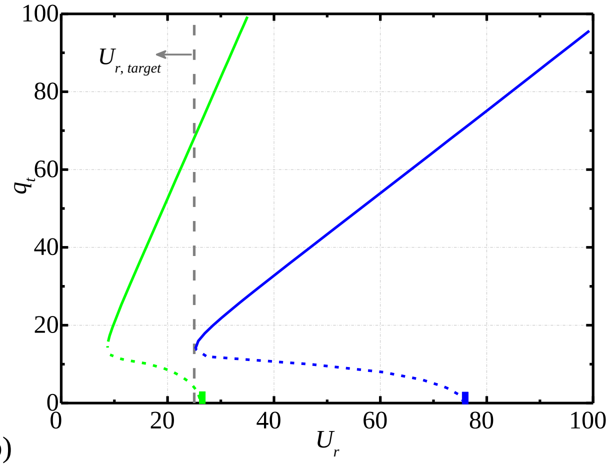


(b)

**Fig. 7.** Case B, galloping behaviors of uncontrolled structure and structure-TMD systems with $R_m$ = 0.3% and 3.0%: (a) $q_s$ versus $U_r$; (b) $q_t$ versus $U_r$. Solid line: stable; dashed line: unstable

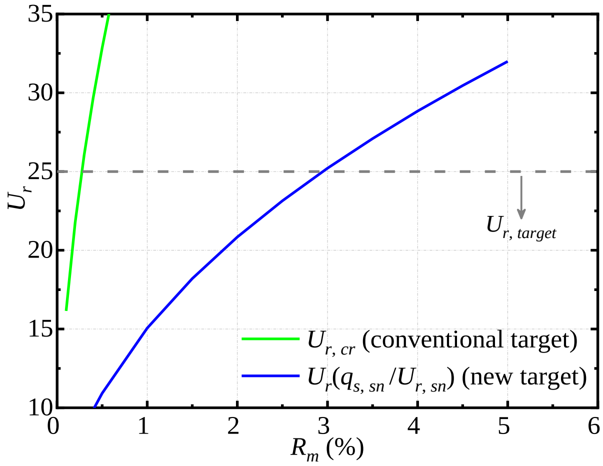


**Fig. 8.** Case B, $U_{r,\ cr}$ and $U_r(q_{s,\ sn}/U_{r,\ sn})$ versus $R_m$

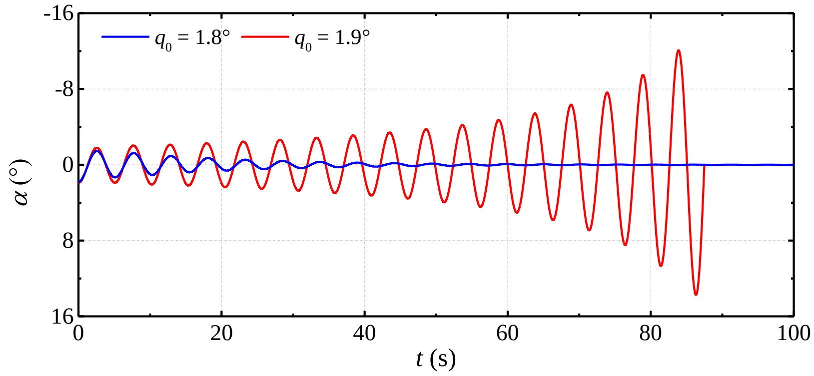


(a)

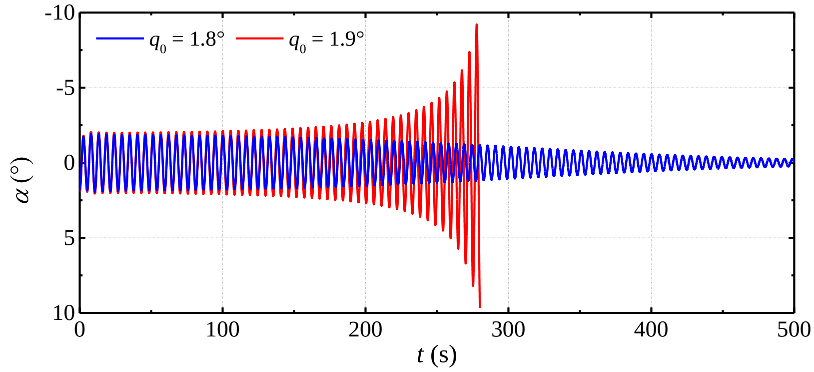


(b)

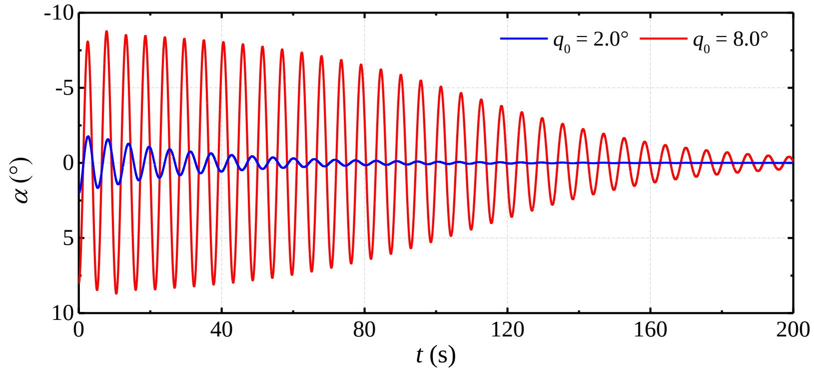


(c)

**Fig. 9.** Case C, displacement histories of a rectangular section: (a) uncontrolled structure at $U$ = 56.0 m/s; (b) structure-TMD system with $R_m$ = 0.56% at $U$ = 61.0 m/s; (c) structure-TMD system with $R_m$ = 3.50% at $U$ = 62.0 m/s

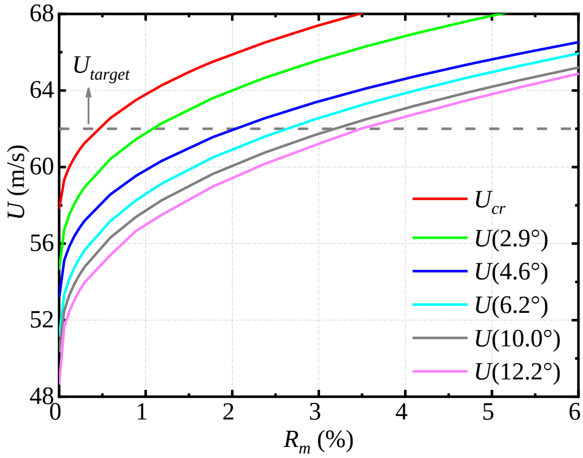


**Fig. 10.** Case C, $U_{cr}$ and $U(q_{\alpha})$ versus $R_m$